Supporting Information for

Water-Restructuring Mutations Can Reverse the Thermodynamic Signature of Ligand Binding to Human Carbonic Anhydrase

Jerome M. Fox[a], Kyungtae Kang[a], Madhavi Sastry[d], Woody Sherman[e], Banumathi Sankaran[f], Peter H. Zwart[f], and George M. Whitesides[a,b,c*]

[a]Department of Chemistry and Chemical Biology, Harvard University

12 Oxford Street, Cambridge, MA 02138, USA.

[b]Wyss Institute for Biologically Inspired Engineering, Harvard University, Cambridge, MA 02138, USA.

[c]The Kavli Institute for Bionano Science and Technology, Harvard University, Cambridge, MA 02138, USA.

[d]Schrödinger, Sanali Infopark, 8-2-120/113 Banjara Hills, Hyderabad 11937, Andhra Pradesh, India

[e]Schrödinger, Inc., 120 West 45th Street, New York, NY 10036, USA.

[f]Berkeley Center for Structural Biology, Lawrence Berkeley National Laboratory, Berkeley, CA, 94720

* To whom correspondence may be addressed: gwhitesides@gmwgroup.harvard.edu

This PDF File includes:
SI Methods
SI Appendices 1-5
SI Figures 1-8
SI Tables 1-9

SI Methods

Mutagenesis. To mutate specific residues of HCAII, we used the Agilent QuickChange Lightening Mutagenesis kit. Using the primers detailed in Table S1, we edited a pACA plasmid containing the gene for HCAII (a kind gift from Carol Fierke and coworkers at the University of Michigan) in accordance with the mutations indicated in Fig. 1.

Production of Human Carbonic Anhydrase II (HCAII). To express HCAII (and mutants of HCAII), we carried out the following steps: (i) We transformed BL21(DE3)pLysS *Escherichia coli* cells with a pACA plasmid and grew the transformed cells on an LB agar plate (100 mg/L Ampicillin) overnight. (ii) We used one colony, thus generated, to inoculate 20 mL of LB broth (25 g/L), and we incubated this culture in a shaker (37°C, 150 rpm) for ~4 h. (iii) Using the 20 mL culture, we inoculated 1 L of rich induction media (20 g/L tryptone, 10 g/L yeast extract, 5 g/L NaCl, 4 g/L M9 salts, 4 g/L glucose, 60μM $ZnSO_4$, and 100 mg/L Ampicillin), and we incubated this culture in a shaker (37°C, 150 rpm) for ~3 h. (iv) At an optical density of ~0.65, we induced expression of HCAII by adding 2.5 mL of a 100-mM solution of isopropyl β-D-1-thiogalactopyranoside and 1.5 mL of a 0.3-M solution of $ZnSO_4$ to the 1 L culture, and we lowered the temperature of the shaker to 25°C. We carried out induction for 12 h. To purify HCAII (and mutants of HCAII), we followed the procedure described by Fierke and coworkers.[1]

Synthesis of Ligands. We synthesized benzo[*d*]thiazole-2-sulfonamide (**BTA**) according to previously published synthetic procedures.[2] We purchased 1,3-thiazole-2-sulfonamide (**TA**) from Enamine, Ltd.

Isothermal Titration Calorimetry (ITC). We carried out all ITC experiments in a Microcal Auto ITC (GE Healthcare) in sodium phosphate buffer (10 mM, pH 7.6, 1-2% DMSO) at 298.15 K. Experiments consisted of 20 injections (8.02 μL) of **BTA** (100-400 μM) into a solution of HCAII (5-20 μM). We used an injection interval of 300 seconds, a stirring speed of 300 rpm, and a reference power of 14 μcal/sec. Using Origin 7.0, we determined K_a and $\Delta H°_{bind}$ by using a nonlinear fit to a single-site model, and we converted these observed values of K_a and $\Delta H°_{bind}$ to pK_a-corrected values of $\Delta G°_{bind}$, $\Delta H°_{bind}$, and $-T\Delta S°_{bind}$ corresponding to the association of Ar-SO_2-NH^- and HCAII-OH_2^+ to form HA-Zn^{2+}-$NHSO_2$-Ar (Table S2) by following the procedure outlined by Snyder et al [2].

For all experiments, we used the following stock solutions of reagents: 20 mM **BTA** (in DMSO) and 50-200 μM HCAII (10 mM sodium phosphate buffer, pH 7.6). To ensure accurate determination of the concentration of protein in stock solutions of HCAII, we carried out the following steps: (i) We estimated the concentration of protein by measuring the absorbance of the stock solution at 280 nm (the extinction coefficient for HCAII is 50,700 cm^{-1} M^{-1}). (ii) We corrected the estimated concentration by carrying out 5 ITC experiments with a standard solution of **BTA**.

With ITC, errors in measurements of $\Delta H°_{bind}$ and K_a translate directly to errors in $\Delta S°_{bind}$ and $\Delta G°_{bind}$ and can, thus, cause *H/S* compensation to be detected where it does not occur (Supplementary Note 1).[3] We carried out three precautionary steps to reduce such errors: (i) We used identical stock solutions of **BTA** and **TA** for each experiment, thereby eliminating changes in the concentration of **BTA** and **TA** between experiments. (ii) We determined values of $\Delta H°_{bind}$ and K_a for the association **BTA** and **TA** with wild-type HCAII before and after determining analogous values for the association or these ligands with mutants, and thus ensured

that wild-type values remained constant throughout the course of our experiments. (iii) We used two independently prepared (i.e., separately expressed and purified) stock solutions of each mutant and a minimum of seven separate ITC runs to determine the enthalpy, entropy, and free energy of binding ($\Delta H°_b$, $-T\Delta S°_b$, and $\Delta G°_b$) for each combination of ligand and mutant.

Protein Crystallization. We prepared monoclinic crystals of HCAII by using the hanging drop vapor diffusion method detailed by Fox et al.[4] We soaked these crystals with **BTA** and **TA** by carrying out the following steps: (i) We prepared soaking solutions containing 1.32 M sodium citrate, 1 mM $ZnSO_4$, 100 mM Tris-HCl (pH 7.8), and 5 mM ligand. (ii) We combined 4 μL of soaking solution and 1-2 crystals of HCAII within a drop on the surface of a reservoir cover (EasyXtal CrystalSupport, Qiagen). (iii) To a clear plastic reservoir in a 15-reservoir plate (EasyXtal, Qiagen), we added 1 mL of soaking solution (without ligand present). We attached the reservoir cover to the reservoir and left the entire setup at 4°C for 1 week.

X-ray Crystallography. All crystallography work was carried out through the Collaborative Crystallography Program of the Berkeley Center for Structural Biology (Lawrence Berkeley National Lab). We collected X-ray diffraction data under a stream of liquid nitrogen at the Advanced Light Source (beams 8.2.1 and 8.2.2).

Solution of Crystal Structures. We solved crystal structures by carrying out the following steps: (i) We performed integration, scaling, and merging of X-ray diffraction data using the xia2 software package.[5] (ii) We analyzed intensity statistics using Phenix.xtriage,[6] a program compatible with the Python-based Hierarchical Environment for Integrated Crystallography (Phenix).[7] (iii) We carried out molecular replacement using PHASER[8] with PDB 3S73 as an

initial search model. (iv) We refined our structures using phenix.refine,[9] and we carried out reciprocal space refinement through several rounds of manual model adjustment in COOT.[10] We calculated the root-mean-square deviation of bond lengths, angles, and dihedrals from ideal geometries using phenix.refine, and we assessed the stereochemical quality of final models using the program MOLPROBITY.[11] Table S5 summarizes the crystallographic details and accession codes (Protein Data Bank; www.rcsb.org) of each X-ray crystal structure.

WaterMap Calculations. We prepared the crystal structures of HCAII (with and without the ligand bound) for WaterMap calculations by using the Protein Preparation Wizard[12] in Maestro (Maestro, version 9.7, Schrödinger, LLC, New York, NY, 2014) to add hydrogens, assign bond orders, optimize hydrogen bonding groups not unambiguously defined by the electron density (e.g., terminal rotamers of Asn, Gln, and His), predict optimal tautomers and ionization states, and optimize the hydrogen bonding network. We then performed a final minimization using the impref refinement module of IMPACT[13] with default settings.

For each HCAII-ligand complex, we carried out WaterMap calculations as described previously.[14–16] Briefly, we performed molecular dynamics simulations using the Desmond MD engine[17] with the OPLS2005 force field.[18–20] Each protein (with and without ligand bound) was solvated with a TIP4P water box extending at least 10.0 Å beyond the protein in all directions, and the default Desmond relaxation protocol was used; this protocol involves successive stages of constrained minimization followed by gradual heating to a temperature of 300 K. After the relaxation step, we performed a 2.0-ns production MD simulation at a temperature of 300 K and pressure of 1 atm with positional restraints (5 kcal/mol/Å^2) on the protein non-hydrogen atoms, extracted molecules of water from 7000 equally spaced snapshots, and subsequently clustered these molecules into distinct hydration sites. We computed the excess

enthalpy (H_{WM}) of water within each hydration site by taking the difference between (i) the average non-bonded interaction energy of waters in each hydration site from the HCAII-ligand MD simulation and (ii) the analogous quantity in the bulk fluid. We computed the excess entropy ($-TS_{WM}$) of water occupying each hydration site by using inhomogeneous solvation theory.[21,22]

To calculate $\Delta J°_{b\text{-}mutant\text{-}WM}$ (where $J = G$, H, or TS), we summed the thermodynamic properties (i.e., G_{WM}, H_{WM}, and TS_{WM}) of hydration sites (located within 12 Å of the position of the bound ligand) in the ligand-bound ($J°_{WM,HCA\text{-}ligand}$) and ligand-free ($J°_{WM,HCA}$) binding pockets. Values of $\Delta J°_{b\text{-}mutant\text{-}WM}$ represent the difference of these two sums ($\Delta J°_{b\text{-}WM} = J°_{WM,HCA\text{-}ligand} - J°_{WM,HCA}$) and, thus, correspond to the association of protein and ligand. Each value $\Delta\Delta J°_{b\text{-}mut\text{-}WM}$ represents the difference in $\Delta J°_{b\text{-}mutant\text{-}WM}$ between a mutant and the wild-type protein ($\Delta\Delta J°_{b\text{-}mut\text{-}WM} = \Delta J°_{b\text{-}mutant\text{-}WM} - \Delta J°_{b\text{-}WT\text{-}WM}$) and, thus, reflects the influence of a specific mutation on the thermodynamics of binding. Each value of $\Delta\Delta J°_{b\text{-}benzo\text{-}WM}$ represents the difference in $\Delta J°_{b\text{-}mutant\text{-}WM}$ between **BTA** and **TA** ($\Delta\Delta J°_{b\text{-}benzo\text{-}WM} = \Delta J°_{b\text{-}\boldsymbol{BTA}\text{-}WM} - \Delta J°_{b\text{-}\boldsymbol{TA}\text{-}WM}$) and, thus, reflects the association of the benzo ring of **BTA** with the nonpolar wall of HCAII.

Alignment. To assess mutation-derived changes in protein structure, we calculated the root-mean-square deviations between each mutant-ligand complex and the wild-type HCAII-**BTA** complex (PDB accession code 3S73)[2]. RMSDs are reported in Table S9.

Docking. For a subset of protein-ligand complexes (**TA** bound to N67Q/L198A, N67QV121T, N67Q/F131Y, and V121T/F131Y, and **BTA** bound to N67Q/L198A and N67Q/F131Y) for which we did not have crystal structures, we used a docking procedure to determine the poses of the bound ligands. We prepared proteins for docking by using the Protein Preparation Wizard (as above). For mutants without crystal structures, we added side chains and predicted the optimal

conformation of those chains by using the Molecular Mechanics/Generalized Born Surface Area (MM/GBSA) approach, as implemented in BioLuminate Residue Scanning.[23] For residues in crystal structures with multiple conformations, we chose the conformation corresponding to the higher occupancy. For N67Q/V121T, the only mutant for which the crystal structure shows a binding site residue (N67Q) with multiple conformations, we performed separate protein preparations for each conformation; for N67/L198A, we did so as well. We performed docking calculations with the SP mode of Glide using default settings.[24,25]

SASA Analysis. We computed solvent-accessible surface areas (SASA) by using the script binding_sasa.py, which is made freely available by the Schrödinger Script Center (www.schrodinger.com/scriptcenter). This approach computes the Connolly surface for both the ligand and receptor, and reports values of surface area in $Å^2$.

Appendices

Appendix 1. H/S Compensation and Experimental Error.

With ITC, errors in measurements of ΔH°_b translate directly to errors in estimates of $-T\Delta S^\circ_b$ (i.e., $-T\Delta S^\circ_b = \Delta G^\circ_b - \Delta H^\circ_b$) and, thus, can cause H/S compensation to be falsely detected. Figure S1A shows an example of such a phenomenon; it plots $-T\Delta S^\circ_b$ against ΔH°_b for 15 measurements of HCAII-**BTA** association. Values of $-T\Delta S^\circ_b$ and ΔH°_b are linearly correlated (R^2 = 0.88, slope = -0.98) and show nearly perfect H/S compensation. When three sets of these 15 measurements—each based on 5 measurements carried out with a separate preparation of wild-type HCAII—are compared against one another, however, they are statistically indistinguishable ($P < 0.01$; Fig. S1B). This result suggests that our experimental precautions (we examined the binding of each ligand to each mutant in at least seven separate experiments carried out with at least two different preparations of protein)—and the statistical significance that they provide—prevent the detection of H/S compensation where it does not occur. Figure S1C plots differences in thermodynamic binding parameters between mutants and wild-type HCAII ($\Delta\Delta J^\circ_{b\text{-}mut} = \Delta J^\circ_{b\text{-}mutant} - \Delta J^\circ_{b\text{-}WT}$, where $J = G$, H, or $-TS$) for every combination of ligand and mutant. Only values that appear small on this plot (e.g., $\Delta\Delta H^\circ_{b\text{-}mut} < 0.50$ kcal/mol) tend to be statistically indistinguishable ($P < 0.01$); large values of $\Delta\Delta J^\circ_{b\text{-}mut}$—those associated with mutations on which we focus our analysis—are statistically significant ($P < 0.01$).

Appendix 2. H/S Compensation for Double and Single Mutants. One important piece of evidence suggests that, in our system, H/S compensation does not arise from experimental error: Most double and triple mutants give rise to changes in enthalpy and entropy of similar or larger magnitudes than single mutants (Fig. S2), indicating that the source of H/S compensation is either preserved or enhanced when mutations are combined. There is no reason for experimental error associated with single mutants to be additive in the context of double or triple mutants; each set of experiments was carried out with a separate set of protein stock solutions.

Appendix 3. Poses of Bound Ligands and WaterMap Calculations. In this study, we collected crystals of ten protein-ligand complexes: nine bound to **BTA** (F131W, V121I, L198A, T199S, V121T, F131Y, N67Q/V121T, F131Y/L198A, and V121T/F131Y) and one bound to **TA** (F131Y/L198A). In these structures, **BTA** had four similar, yet distinct poses—though, no more than two in any given structure (Figs. S4 and S7, Table S6); **TA** showed two distinct poses. Because crystal structures were determined under cryogenic conditions (77 K), the ligand poses that they reveal do not necessarily correspond to the poses of bound ligands in our calorimetric studies (carried out at 298.15 K); nonetheless, we used crystallographically determined poses as a best guess of poses at room temperature. For most mutant/ligand combinations in Figs. 2B and S5 (specifically, eight out of ten of those examined if Fig. 2C, and nine out of twelve of those examined in Fig. S5), values of $\Delta\Delta J°_{b\text{-}mut\text{-}WM}$ are based on the highest occupancy pose of a ligand (in either the crystal structure or docked structure of the relevant mutant-ligand complex); for a small subset of mutant/ligand combinations, however, values of $\Delta\Delta J°_{b\text{-}mut\text{-}WM}$ are based on either a secondary ligand pose (i.e., a lower occupancy pose in the corresponding crystal structure or a related structure; examples include **BTA** bound to T199S and L198A/F131Y in Fig. 2B, and **BTA** bound to L198A/F131Y and **TA** bound to L198A/F131Y and N67Q/L198A in Fig. S5) or a secondary side chain pose (i.e., Q67 in N67Q/V121T in Fig. 2C, and Q67 in both N67Q/V121T and N67Q/L198A in Fig. S5). Secondary poses were used when they yielded significantly better agreement between $\Delta\Delta J°_{b\text{-}mut}$ and $\Delta\Delta J°_{b}$ than primary poses; accordingly, the similarity in trends between values of $\Delta\Delta J°_{b\text{-}mut}$ and $\Delta\Delta J°_{b\text{-}mut\text{-}WM}$ suggests that rearrangements of water (the only influence for which WaterMap calculations account) are a plausible cause of these trends.

Crystal structures of N67Q/F131Y show **TA** bound with two poses (Fig. S7). The first, which has a slightly higher occupancy than the second, has the same orientation as bound **BTA**;

the second is rotated 90° to the first. Differences in thermodynamic parameters of **BTA** and **TA** could, thus, include contributions from the rotation of the thiazole ring of **TA** from the first pose to the second. These contributions represent a potential source of error in our analysis.

Appendix 4. Direct hydrogen bonds. The sulfonamide moiety of **BTA** and **TA** participates in hydrogen bonds with the amide nitrogen and side-chain hydroxyl of threonine 199. Our crystal structures indicate that the position of the sulfonamide is unperturbed across mutants, suggesting that the thermodynamic influence of sulfonamide-mediated hydrogen bonds between the ligand and protein is insensitive to mutations.

Appendix 5. SASA and Free Energy. To determine if differences in HCAII-ligand contact area might—perhaps, by affecting van der Waals interactions or the structural flexibility of the protein-ligand complex—cause differences in the thermodynamics of binding, we plotted $\Delta G°_{b\text{-}\boldsymbol{BTA}}$ against $\Delta SASA_{bind\text{-}ligand}$, the loss in solvent accessible surface area of the ligand that occurs during binding (i.e., $\Delta SASA_{bind\text{-}ligand} = SASA_{ligand\text{-}free} - SASA_{ligand\text{-}bound}$) for single mutants for which we had crystal structures (Fig. S8). Interestingly, values of $\Delta SASA_{bind\text{-}ligand}$ differed by less than 21Å^2 between mutants and showed no correlation—linear or otherwise—with $\Delta G°_{b\text{-}\boldsymbol{BTA}}$; values of $\Delta SASA_{bind\text{-}ligand}$ for L198A and F131Y, for example, differ by 21Å^2, yet these two mutants have free energies of binding that are statistically indistinguishable ($P < 0.01$). The lack of an obvious correlation between $\Delta SASA_{bind\text{-}ligand}$ and $\Delta G°_{b\text{-}\boldsymbol{BTA}}$ suggests that mutation-derived changes in protein-ligand contact area—through van der Waals interactions or other influences—are not the primary cause of differences in binding affinity between mutants.

Supplementary Figures

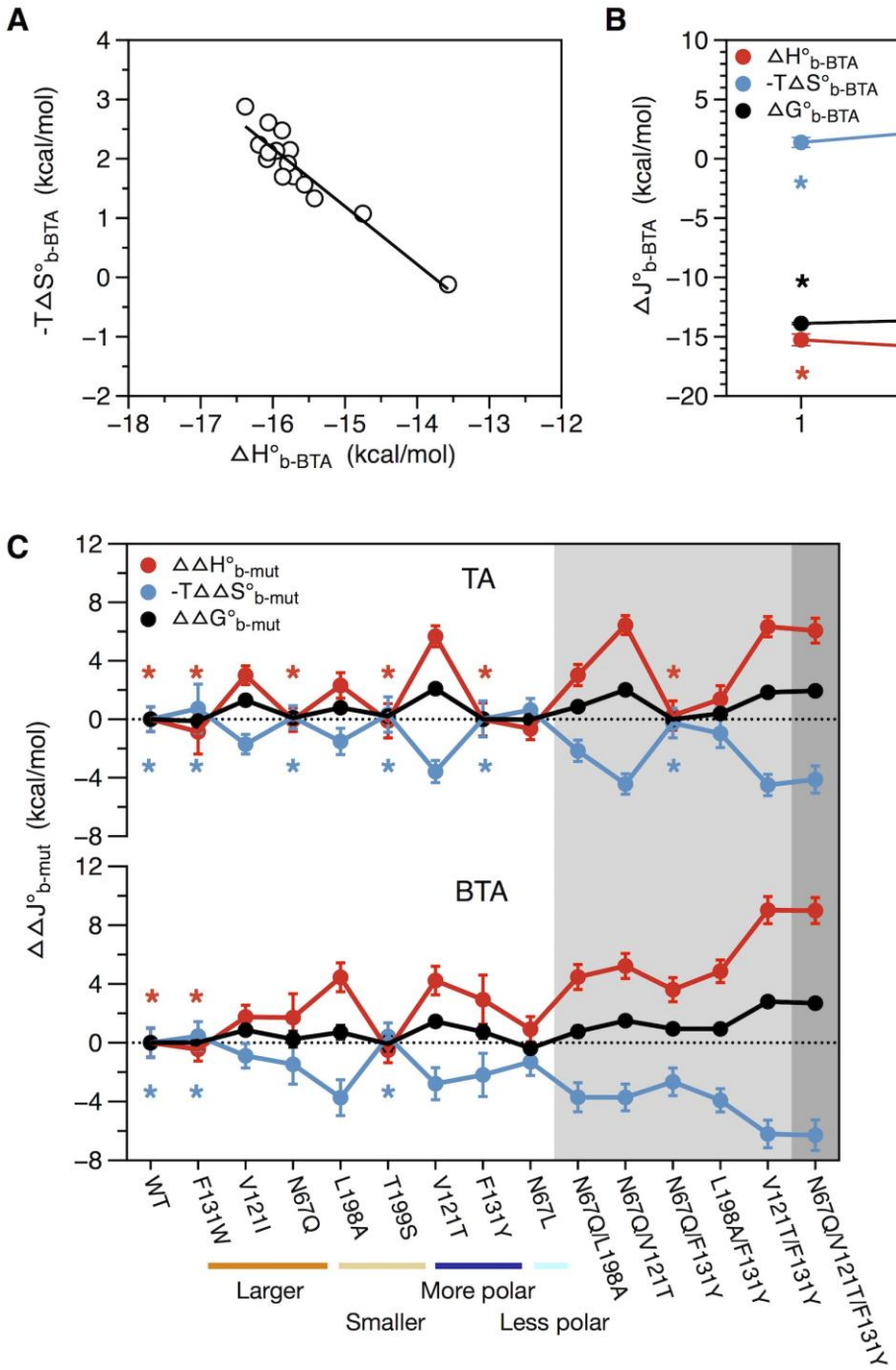

Figure S1. Statistical analysis of H/S compensation. (A) A plot of the entropy ($-T\Delta S°_{b\text{-}BTA}$) and enthalpy ($\Delta H°_{b\text{-}BTA}$) of binding for **BTA** and wild-type HCAII. The line represents a linear fit to the data (R^2 = 0.88, slope = -0.98), and shows nearly perfect H/S compensation that arises from

experimental error. (B) A plot showing three estimates of thermodynamic binding parameters for **BTA**; each represents the average of five individual measurements carried out with a separate preparation of wild-type HCAII. Error bars represent standard error ($n \geq 5$). (C). Differences in the thermodynamic binding parameters of mutants and wild-type HCAII: $\Delta\Delta J°_{b\text{-}mut} = \Delta J°_{b\text{-}mutant} - \Delta J°_{b\text{-}WT}$ (where $J = G$, H, or $-TS$). Error bars represent standard deviation ($n \geq 7$). For (B-C), asterisks (*) indicate values that are statistically indistinguishable ($P < 0.01$). Thus, apparent differences in values of $\Delta\Delta J°_{b\text{-}mut}$ between mutants are statistically significant ($P < 0.01$); apparent differences in values of $\Delta J°_{b\text{-}BTA}$ between preparations of wild-type HCAII are not.

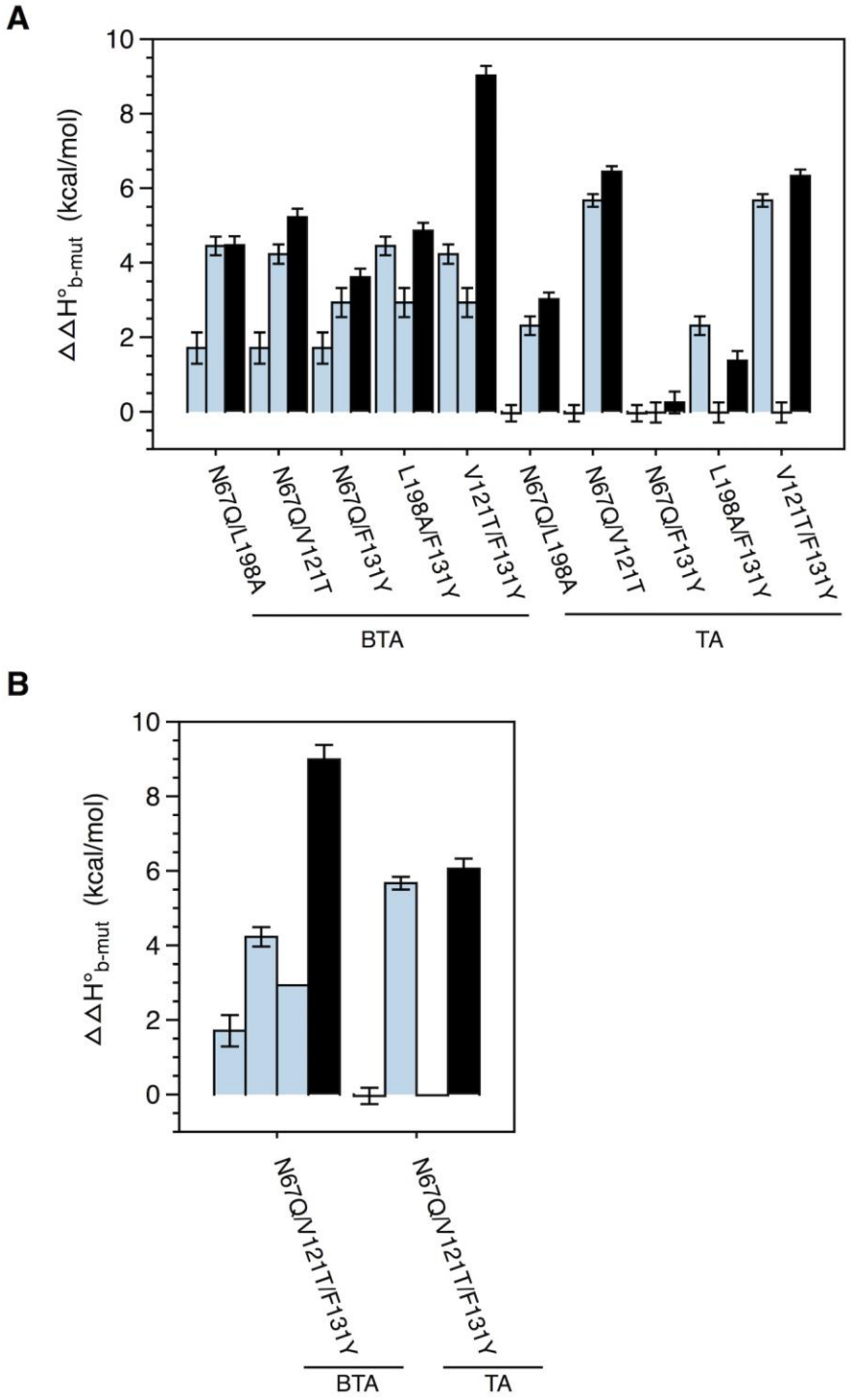

Figure S2. H/S Compensation associated with double and single mutants. Bar graphs showing the influence of (A) double and (B) triple mutations on the enthalpies of binding (i.e., $\Delta\Delta H°_{b\text{-}mut} = \Delta H°_{b\text{-}mut} - \Delta H°_{b\text{-}WT}$) for both ligands. Black bars represent values of $\Delta\Delta H°_{b\text{-}mut}$ for double or triple mutants; blue bars represent values of $\Delta\Delta H°_{b\text{-}mut}$ for the corresponding single mutants. For

double or triple mutants (with one exception—the binding of **TA** to L198A/F131Y), values of $\Delta\Delta H°_{b\text{-}mut}$ are equal to or larger than corresponding values for single mutants; we would not expect such a relationship if H/S compensation was the result of experimental error.

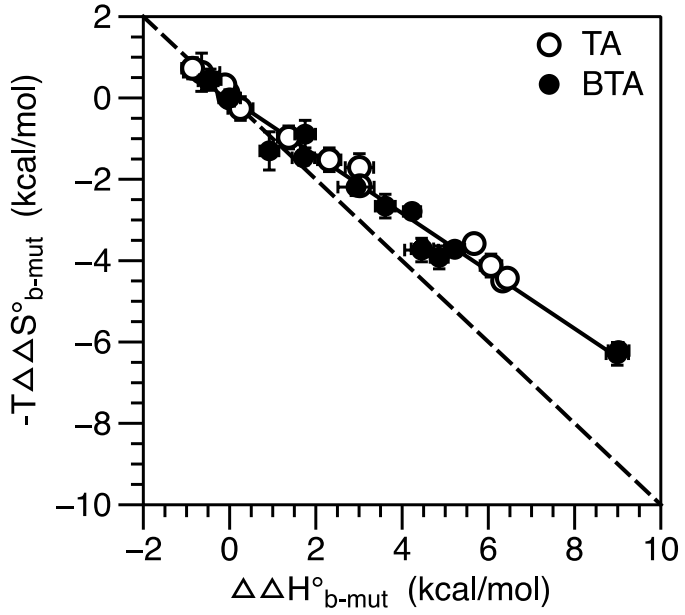

Figure S3. The relationship between the enthalpic and entropic influence of mutations. The dashed line represents perfect compensation ($-T\Delta\Delta S°_{b\text{-}mut} = -\Delta\Delta H°_{b\text{-}mut}$). Values of $\Delta\Delta H°_{b\text{-}mut}$ and $-T\Delta\Delta S°_{b\text{-}mut}$ are linearly correlated (slope = -0.71 and $R^2 = 0.98$) for both ligands (error bars represent standard error; $n \geq 7$).

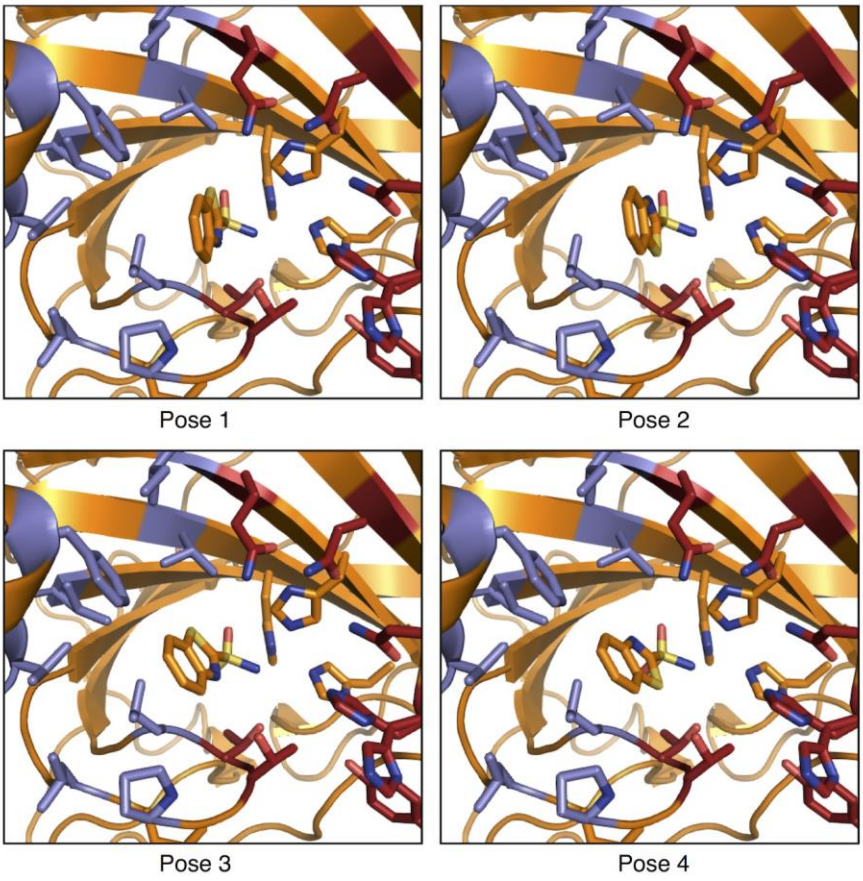

Figure S4. Poses of bound **BTA**. In crystal structures of mutant-ligand complexes, **BTA** had one of four distinct poses (summarized in Table S6): Pose 1 (Wild-type, F121W, V121I*, L198A, T199S, F131Y, V121T/N67, and V121T/F131Y), Pose 2 (V121I), Pose 3 (L198A*, V121T*, F131Y/L198A), and Pose 4 (V121T). In these annotations, asterisks indicate the primary pose (highest occupancy).

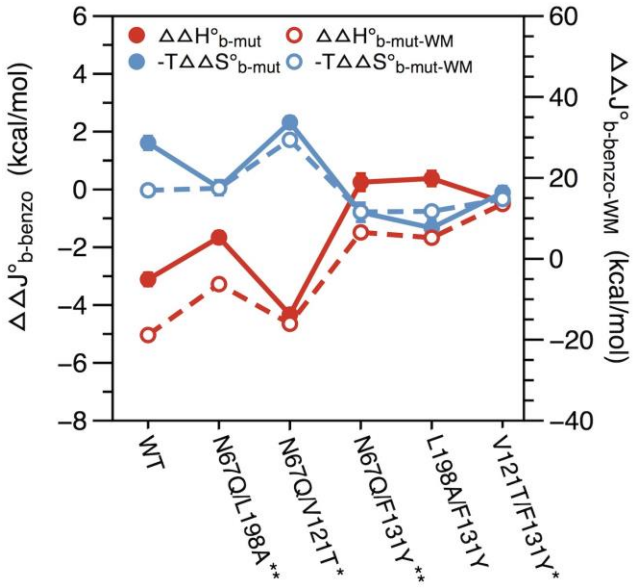

Figure S5. A comparison of values of $\Delta\Delta J°_{b\text{-}benzo}$ (J = G, H, or TS) determined using ITC and WaterMap. (Error bars represent standard error; n ≥ 7). We used X-ray crystal structures for WaterMap calculations except where indicated: For mutants marked *, we used an X-ray crystal structure of the HCAII-**BTA** complex and a modeled structure of the HCAII-**TA** complex; for those marked **, we modeled the structures of both HCAII-ligand complexes. See Docking in SI Methods.

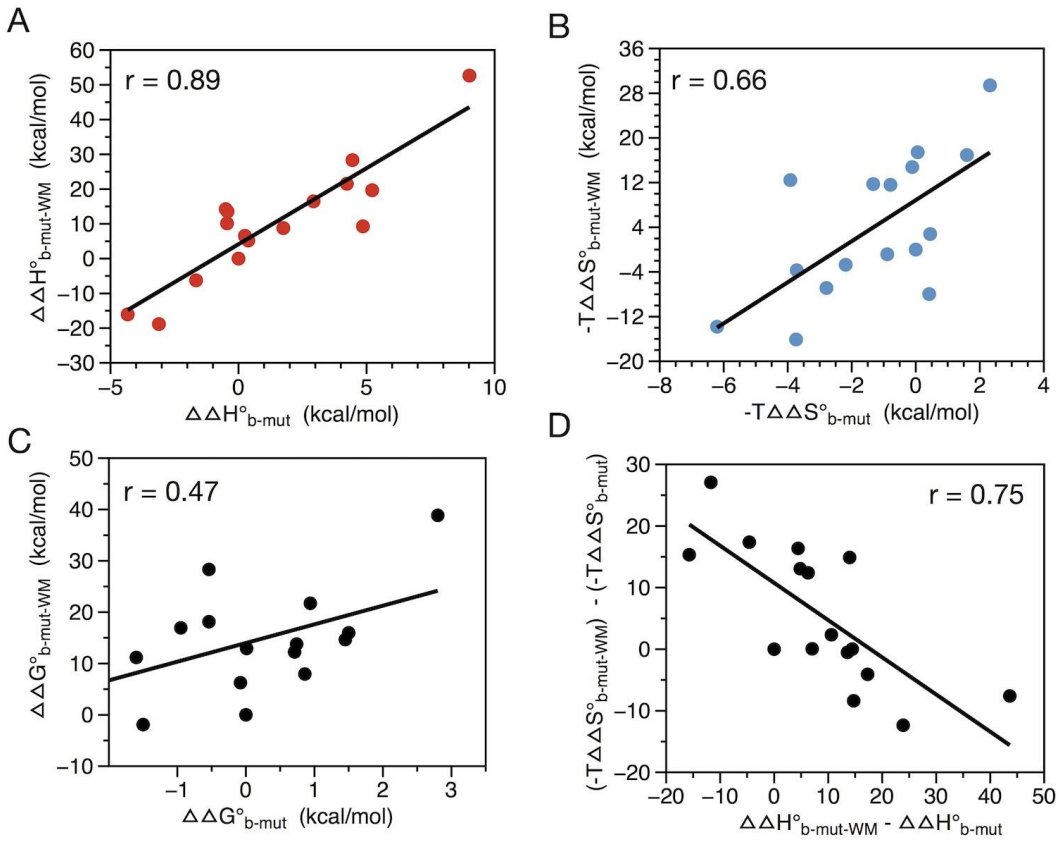

Figure S6. A comparison of ITC- and WaterMap-based estimates of mutation derived changes in (A) enthalpy, (B) entropy, and (C) free energy of binding. Data correspond to values of $\Delta\Delta J°_{b\text{-}mut}$ plotted in Figure 2B and values of $\Delta\Delta J°_{b\text{-}benzo}$ plotted in Figure S5. Correlation coefficients, t statistics, and two-tailed probabilities associated with these correlations are shown in Table S10. Correlations are strong[26] ($P < 0.01$) for both enthalpy and entropy, but weak for free energy ($P = 0.06$), evidencing (D) a correlation between discrepancies in enthalpy and entropy ($P < 0.01$). Such a correlation may be the result of inaccuracies associated with crystallographically determined conformations of the ligand and/or neighboring residues; such conformations, if evenly slightly incorrect, would affect estimates of both enthalpy and entropy.

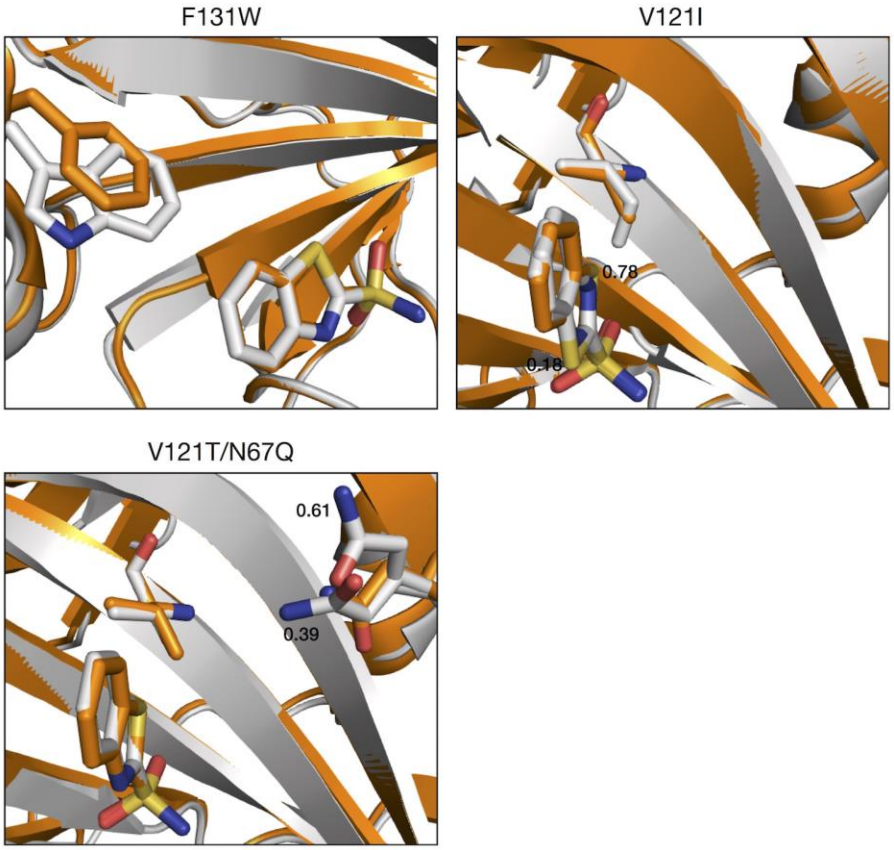

Figure S7. A comparison of the orientation of (i) mutations that increase the size of side chains and (ii) corresponding wild-type residues. The wild-type structure appears in orange; mutant structures, in white. Numerical insets correspond to occupancies of **BTA** in V121I (as detailed in Fig. S4 and Table S6) and glutamine 67 in V121T/N67Q.

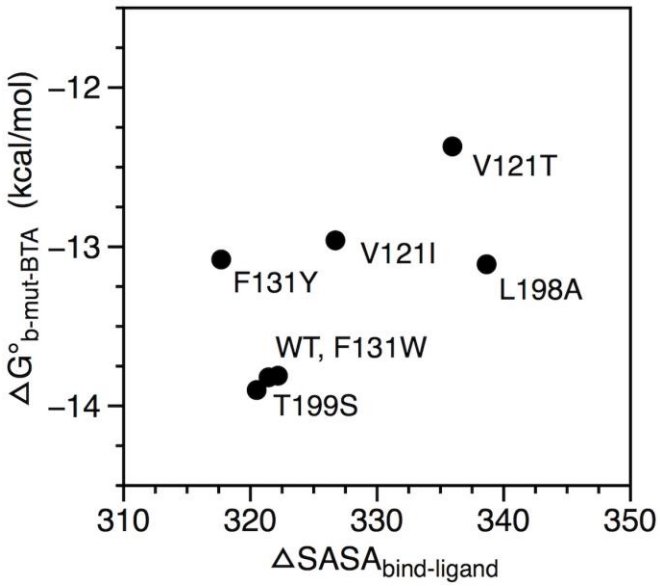

Figure S8. The influence of buried surface area on the thermodynamics of binding. A plot showing the relationship between $\Delta G°_{b\text{-}\boldsymbol{BTA}}$ and $\Delta SASA_{bind\text{-}ligand}$, the loss in solvent accessible surface area of the ligand that occurs during binding (i.e., $\Delta SASA_{bind\text{-}ligand} = SASA_{ligand\text{-}free} - SASA_{ligand\text{-}bound}$). A correlation coefficient, t statistic, and two-tailed probability associated with a linear correlation of this data is shown in Table S8; the correlation is not statistically significant ($P < 0.01$).

Supplementary Tables

Table S1. Primers for mutagenesis.

Mutation	*Forward primer*	*Reverse primer*
Phe131Trp	TGG AAC ACC AAA TAT GGG GAT TGG GGG AAA GCT GTG CAG CAA CCT	AGG TTG CTG CAC AGC TTT CCC CCA ATC CCC ATA TTT GGT GTT CCA
Val121Ile	TAT GCT GCA GAA CTT CAC TTG ATT CAC TGG AAC ACC AAA TAT GGG	CCC ATA TTT GGT GTT CCA GTG AAT CAA GTG AAG TTC TGC AGC ATA
Asn67Gln	CTC AAC AAT GGT CAT GCT TTC CAG GTG GAG TTT GAT GAC TCT CAG	CTG AGA GTC ATC AAA CTC CAC CTG GAA AGC ATG ACC ATT GTT GAG
Leu198Ala	TAC TGG ACC TAC CCA GGC TCA GCC ACC ACC CCT CCT CTT CTG GAA	TTC CAG AAG AGG AGG GGT GGT GGC TGA GCC TGG GTA GGT CCA GTA
Thr199Ser	TGG ACC TAC CCA GGC TCA CTG AGC ACC CCT CCT CTT CTG GAA TGT	ACA TTC CAG AAG AGG AGG GGT GCT CAG TGA GCC TGG GTA GGT CCA
Val121Thr	TAT GCT GCA GAA CTT CAC TTG ACT CAC TGG AAC ACC AAA TAT GGG	CCC ATA TTT GGT GTT CCA GTG AGT CAA GTG AAG TTC TGC AGC ATA
Phe131Tyr	TGG AAC ACC AAA TAT GGG GAT TAT GGG AAA GCT GTG CAG CAA CCT	AGG TTG CTG CAC AGC TTT CCC ATA ATC CCC ATA TTT GGT GTT CCA
Asn67Leu	CTC AAC AAT GGT CAT GCT TTC CTG GTG GAG TTT GAT GAC TCT CAG	CTG AGA GTC ATC AAA CTC CAC CAG GAA AGC ATG ACC ATT GTT GAG

Table S2. pK_a-corrected thermodynamic binding parameters.

Mutant	*Ligand*	*Samples (ITC runs)*	*n*	K_d (nM)	ΔG°_b (kcal/mol)	ΔH°_b (kcal/mol)	$-T\Delta S^\circ_b$ (kcal/mol)
WT	TA	20	1.00	0.93 (0.10)	-12.32 (0.01)	-12.56 (0.13)	0.24 (0.14)
Phe131Trp	TA	12	1.03	0.81 (0.31)	-12.45 (0.08)	-13.42 (0.40)	0.97 (0.45)
Val121Ile	TA	12	0.99	8.40 (0.65)	-11.02 (0.01)	-9.55 (0.07)	-1.47 (0.08)
Asn67Gln	TA	10	1.03	1.10 (0.18)	-12.23 (0.03)	-12.60 (0.17)	0.37 (0.16)
Leu198Ala	TA	9	0.97	3.58 (0.62)	-11.53 (0.03)	-10.25 (0.21)	-1.28 (0.22)
Thr199Ser	TA	11	1.00	1.34 (0.26)	-12.11 (0.03)	-12.67 (0.31)	0.56 (0.32)
Val121Thr	TA	16	0.92	32.04 (4.48)	-10.23 (0.02)	-6.89 (0.10)	-3.34 (0.11)
Phe131Tyr	TA	17	1.01	0.99 (0.32)	-12.31 (0.05)	-12.58 (0.23)	0.26 (0.26)
Asn67Leu	TA	12	0.94	0.90 (0.11)	-12.35 (0.02)	-13.21 (0.13)	0.87 (0.14)
Asn67Gln / Leu198Ala	TA	11	1.04	4.01 (0.61)	-11.46 (0.03)	-9.54 (0.13)	-1.92 (0.12)
Val121Thr / Asn67Gln	TA	11	0.93	27.87 (3.96)	-10.31 (0.03)	-6.12 (0.08)	-4.19 (0.10)
Phe131Tyr / Asn67Gln	TA	10	1.07	0.94 (0.21)	-12.33 (0.04)	-12.31 (0.25)	-0.02 (0.26)
Phe131Tyr / Leu198Ala	TA	10	1.03	1.92 (0.78)	-11.93 (0.07)	-11.19 (0.22)	-0.73 (0.24)
Val121Thr / Phe131Tyr	TA	10	0.98	20.94 (2.86)	-10.48 (0.03)	-6.23 (0.12)	-4.26 (0.13)
Val121Thr / Phe131Tyr / Asn67Gln	TA	8	0.92	24.87 (4.34)	-10.38 (0.04)	-6.50 (0.21)	-3.88 (0.25)
WT	BTA	15	1.00	0.08 (0.04)	-13.82 (0.06)	-15.67 (0.18)	1.85 (0.19)
Phe131Trp	BTA	11	1.07	0.09 (0.06)	-13.81 (0.10)	-16.12 (0.12)	2.30 (0.20)
Val121Ile	BTA	17	1.00	0.32 (0.06)	-12.96 (0.02)	-13.92 (0.10)	0.96 (0.10)
Asn67Gln	BTA	15	1.00	0.15 (0.13)	-13.58 (0.12)	-13.96 (0.38)	0.38 (0.29)
Leu198Ala	BTA	16	1.02	0.29 (0.16)	-13.11 (0.10)	-11.22 (0.18)	-1.89 (0.25)
Thr199Ser	BTA	10	1.00	0.08 (0.04)	-13.90 (0.13)	-16.17 (0.16)	2.27 (0.19)
Val121Thr	BTA	14	1.01	0.90 (0.25)	-12.37 (0.06)	-11.44 (0.18)	-0.94 (0.22)
Phe131Tyr	BTA	19	1.00	0.31 (0.20)	-13.08 (0.09)	-12.74 (0.35)	-0.34 (0.29)
Asn67Leu	BTA	12	0.99	0.04 (0.01)	-14.20 (0.05)	-14.75 (0.15)	0.55 (0.17)
Asn67Gln / Leu198Ala	BTA	10	1.04	0.29 (0.11)	-13.06 (0.09)	-11.20 (0.16)	-1.86 (0.21)
Val121Thr / Asn67Gln	BTA	11	1.00	0.95 (0.23)	-12.32 (0.04)	-10.45 (0.15)	-1.87 (0.17)
Phe131Tyr / Asn67Gln	BTA	10	0.98	0.39 (0.15)	-12.87 (0.07)	-12.06 (0.14)	-0.81 (0.19)
Phe131Tyr / Leu198Ala	BTA	10	0.99	0.37 (0.08)	-12.88 (0.04)	-10.81 (0.11)	-2.07 (0.11)
Val121Thr / Phe131Tyr	BTA	11	0.96	8.62 (2.14)	-11.02 (0.05)	-6.65 (0.18)	-4.36 (0.18)
Val121Thr / Phe131Tyr / Asn67Gln	BTA	8	1.02	7.40 (2.65)	-11.13 (0.08)	-6.68 (0.19)	-4.44 (0.26)

*Errors represent standard error ($n \geq 7$).

Table S3. The influence of mutations on thermodynamic binding parameters.

Mutant	*Ligand*	$\Delta\Delta G^{\circ}_{b\text{-}mut}$ *(kcal/mol)*	$\Delta\Delta H^{\circ}_{b\text{-}mut}$ *(kcal/mol)*	$-T\Delta\Delta S^{\circ}_{b\text{-}mut}$ *(kcal/mol)*
WT	TA	0.00 (0.02)	0.00 (0.19)	0.00 (0.20)
Phe131Trp	TA	-0.13 (0.08)	-0.86 (0.42)	0.73 (0.47)
Val121Ile	TA	1.30 (0.02)	3.01 (0.15)	-1.71 (0.16)
Asn67Gln	TA	0.09 (0.03)	-0.04 (0.22)	0.13 (0.21)
Leu198Ala	TA	0.79 (0.03)	2.31 (0.25)	-1.52 (0.26)
Thr199Ser	TA	0.21 (0.04)	-0.11 (0.33)	0.32 (0.34)
Val121Thr	TA	2.09 (0.02)	5.67 (0.17)	-3.58 (0.18)
Phe131Tyr	TA	0.01 (0.05)	-0.02 (0.27)	0.02 (0.29)
Asn67Leu	TA	-0.03 (0.02)	-0.65 (0.19)	0.63 (0.20)
Asn67Gln / Leu198Ala	TA	0.86 (0.03)	3.02 (0.18)	-2.16 (0.19)
Val121Thr / Asn67Gln	TA	2.01 (0.03)	6.44 (0.15)	-4.43 (0.17)
Phe131Tyr / Asn67Gln	TA	-0.01 (0.04)	0.25 (0.29)	-0.26 (0.29)
Phe131Tyr / Leu198Ala	TA	0.39 (0.07)	1.37 (0.26)	-0.97 (0.28)
Val121Thr / Phe131Tyr	TA	1.84 (0.03)	6.33 (0.17)	-4.50 (0.19)
Val121Thr / Phe131Tyr / Asn67Gln	TA	1.94 (0.04)	6.06 (0.25)	-4.12 (0.28)
WT	BTA	0.00 (0.09)	0.00 (0.25)	0.00 (0.27)
Phe131Trp	BTA	0.01 (0.11)	-0.45 (0.22)	0.45 (0.28)
Val121Ile	BTA	0.86 (0.06)	1.75 (0.20)	-0.89 (0.21)
Asn67Gln	BTA	0.24 (0.14)	1.71 (0.42)	-1.47 (0.35)
Leu198Ala	BTA	0.71 (0.12)	4.45 (0.25)	-3.74 (0.31)
Thr199Ser	BTA	-0.08 (0.14)	-0.50 (0.24)	0.42 (0.27)
Val121Thr	BTA	1.45 (0.09)	4.23 (0.26)	-2.79 (0.29)
Phe131Tyr	BTA	0.74 (0.11)	2.93 (0.39)	-2.19 (0.35)
Asn67Leu	BTA	-0.38 (0.08)	0.92 (0.23)	-1.30 (0.26)
Asn67Gln / Leu198Ala	BTA	0.76 (0.11)	4.47 (0.24)	-3.71 (0.29)
Val121Thr / Asn67Gln	BTA	1.50 (0.07)	5.22 (0.23)	-3.72 (0.26)
Phe131Tyr / Asn67Gln	BTA	0.95 (0.09)	3.61 (0.23)	-2.66 (0.27)
Phe131Tyr / Leu198Ala	BTA	0.94 (0.07)	4.86 (0.21)	-3.92 (0.22)
Val121Thr / Phe131Tyr	BTA	2.80 (0.08)	9.02 (0.26)	-6.21 (0.26)
Val121Thr / Phe131Tyr / Asn67Gln	BTA	2.69 (0.10)	8.99 (0.26)	-6.29 (0.33)

*Errors represent standard error ($n \geq 7$).

Table S4. Thermodynamic binding parameters corresponding to the association of the benzo group of BTA with the nonpolar wall of HCAII.

Mutant	*Ligand*	$\Delta\Delta G^{\circ}_{b\text{-}benzo}$ *(kcal/mol)*	$\Delta\Delta H^{\circ}_{b\text{-}benzo}$ *(kcal/mol)*	$-T\Delta\Delta S^{\circ}_{b\text{-}benzo}$ *(kcal/mol)*
WT	BTA-TA	-1.50 (0.07)	-3.11 (0.22)	1.61 (0.23)
Phe131Trp	BTA-TA	-1.36 (0.13)	-2.69 (0.42)	1.33 (0.49)
Val121Ile	BTA-TA	-1.94 (0.03)	-4.37 (0.12)	2.43 (0.13)
Asn67Gln	BTA-TA	-1.35 (0.13)	-1.36 (0.42)	0.01 (0.33)
Leu198Ala	BTA-TA	-1.58 (0.10)	-0.98 (0.28)	-0.60 (0.33)
Thr199Ser	BTA-TA	-1.78 (0.14)	-3.50 (0.35)	1.71 (0.37)
Val121Thr	BTA-TA	-2.15 (0.06)	-4.55 (0.21)	2.40 (0.24)
Phe131Tyr	BTA-TA	-0.77 (0.10)	-0.17 (0.42)	-0.61 (0.39)
Asn67Leu	BTA-TA	-1.85 (0.05)	-1.53 (0.20)	-0.32 (0.22)
Asn67Gln / Leu198Ala	BTA-TA	-1.60 (0.09)	-1.66 (0.20)	0.06 (0.25)
Val121Thr / Asn67Gln	BTA-TA	-2.01 (0.05)	-4.33 (0.17)	2.32 (0.20)
Phe131Tyr / Asn67Gln	BTA-TA	-0.54 (0.08)	0.25 (0.29)	-0.79 (0.32)
Phe131Tyr / Leu198Ala	BTA-TA	-0.95 (0.08)	0.38 (0.25)	-1.33 (0.26)
Val121Thr / Phe131Tyr	BTA-TA	-0.54 (0.05)	-0.43 (0.22)	-0.11 (0.22)
Val121Thr / Phe131Tyr / Asn67Gln	BTA-TA	-0.75 (0.09)	-0.19 (0.29)	-0.56 (0.36)

*Errors represent standard error ($n \geq 7$).

Table S5. Crystallographic data for HCAII-ligand complexes of various mutants.

	F131W-BTA	***V121I-BTA***	***L198A-BTA***	***T199S-BTA***	***V121T-BTA***
Accession code (www.rcsb.org)	5JDV	5JEG	5JEH	5JEP	5JES
Data collection and processing					
No. crystals analyzed	1	1	1	1	1
Wavelength	1.100 Å	1.100 Å	1.100 Å	1.100 Å	1.100 Å
Space group	$P12_11$	$P12_11$	$P12_11$	$P12_11$	$P12_11$
Unit cell parameters					
a	42.34	42.43	42.08	42.57	42.08
b	41.68	41.48	41.28	41.28	41.28
c	72.78	72.64	72.05	72.82	75.05
α	90.00	90.00	90.00	90.00	90.00
β	104.67	104.64	104.41	104.75	104.41
γ	90.00	90.00	90.00	90.00	90.00
Diffraction data					
High resolution bin	1.36-1.34	1.20-1.19	1.14-1.13	1.21-1.19	1.22-1.20
# of reflections	1469	4886	4690	2245	1438
Refinement					
Resolution range	35.22-1.34	35.74-1.19	35.55-1.13	70.54-1.19	34.91-1.20
Completeness	86.02	98.25	92.69	88.31	81.25
R(work)	0.136	0.132	0.129	0.123	0.121
R(free)	0.169	0.156	0.159	0.148	0.147
B(avg)	13.1	14.6	15.2	12.4	17.1
Bond lengths	0.011	0.016	0.021	0.010	0.010
Bond angles	1.349	2.214	2.003	1.373	1.774
Protein residues	259	260	260	259	259
Zinc ions	1	1	1	1	1
Water molecules*	438	396	424	459	374
Ligands (BTA or TA)**	1	4	1	2	4

*This number denotes the number of water molecules observed in the crystal structure (inside the binding pocket and exterior to the protein).

**This number denotes the number of ligands and ligand poses observed in the crystal structure. In addition to appearing inside the binding pocket, ligands often also appear at a site on the exterior of the protein, an artifact of crystallography.

***Crystal structures are available in the Protein Data Bank (www.rcsb.org).

Table S5 (cont.). Crystallographic data for HCAII-ligand complexes of various mutants.

	F131Y-BTA	***V121T/ N67Q-BTA***	***V121T/ F131Y-BTA***	***F131Y/ L198A-BTA***	***F131Y/ L198A-TA***
Accession code (www.rcsb.org)	5JE7	5JG3	5JG5	5JGS	5JGT
Data collection and processing					
No. crystals analyzed	1	1	1	1	1
Wavelength	1.100 Å	1.100 Å	1.100 Å	1.100 Å	1.100 Å
Space group	$P12_11$	$P12_11$	$P12_11$	$P12_11$	$P12_11$
Unit cell parameters					
a	42.48	42.47	42.43	42.35	42.41
b	41.72	41.69	41.68	41.88	41.47
c	72.57	73.08	72.33	72.06	72.39
α	90.00	90.00	90.00	90.00	90.00
β	104.71	104.74	104.71	104.63	104.60
γ	90.00	90.00	90.00	90.00	90.00
Diffraction data					
High resolution bin	1.16-1.15	1.23-1.21	1.21-1.19	1.12-1.11	1.11-1.10
# of reflections	1459	3210	2946	250	813
Refinement					
Resolution range	25.44-1.15	35.92-1.21	30.76-1.19	40.04-1.11	40.12-1.10
Completeness	84.74	91.69	91.77	74.65	75.80
R(work)	0.122	0.132	0.121	0.119	0.119
R(free)	0.144	0.152	0.141	0.131	0.138
B(avg)	17.1	14.9	13.7	13.8	12.1
Bond lengths	0.010	0.010	0.011	0.011	0.011
Bond angles	1.368	1.335	1.345	1.364	1.374
Protein residues	258	260	260	258	260
Zinc ions	1	1	1	1	1
Water molecules*	462	417	445	444	425
Ligands (BTA or TA)**	2	3	3	3	4

*This number denotes the number of water molecules observed in the crystal structure (inside the binding pocket and exterior to the protein).

**This number denotes the number of ligands and ligand poses observed in the crystal structure. In addition to appearing inside the binding pocket, ligands often also appear at a site on the exterior of the protein, an artifact of crystallography.

***Crystal structures are available in the Protein Data Bank (www.rcsb.org).

Table S6. Poses of BTA in different mutants.

Pose 1	*Pose 2*	*Pose 3*	*Pose 4*
WT, F131W, V121I*, L198A, T199S, F131Y, V121T/N67Q, V121T/F131Y	V121I	L198A*, V121T*, F131Y/L198A	V121T

*Denotes primary pose (highest occupancy).

**Poses correspond to those indicated in Fig. S4.

Table S7. Changes in the hydrophilicity and volume of side chains caused by amino acid substitutions

Amino acid	*Hopp-Woods index*[27]	*Volume ($Å^3$)*[28]	*Mutation*	*Diff P*	*ΔP (norm)*	*Diff V*	*ΔV (norm)*
Ala	-0.5	88.6	WT	0.00	0.000	0.00	0.000
Arg	3	173.4	Asn67Gln	0.00	0.000	37.9	0.227
Asn	0.2	114.1	Thr199Ser	0.70	0.212	26.7	-0.207
Asp	3	111.1	Asn67Leu	-2.00	-0.606	29.7	0.402
Cys	-1	108.5	Phe131Trp	-0.90	-0.273	-78.1	0.290
Gln	0.2	143.8	Val121Ile	-0.30	-0.091	-27.1	0.204
Glu	3	138.4	Leu198Ala	1.30	0.394	-23.9	-0.598
Gly	0	60.1	Val121Thr	1.10	0.333	3.7	-0.183
His	-0.5	153.2	Phe131Tyr	0.20	0.061	52.6	0.028
Ile	-1.8	166.7					
Leu	-1.8	166.7					
Lys	3	168.6					
Met	-1.3	162.9					
Phe	-2.5	189.9					
Pro	0	112.7					
Ser	0.3	89					
Thr	-0.4	116.1					
Trp	-3.4	227.8					
Tyr	-2.3	193.6					
Val	-1.5	140					

* For the Hopp-Woods index, *more* positive implies *more* hydrophilic.

**Values of ΔP and ΔV were normalized to have a range of unity. This identical range enables informative comparisons of values of w_p and w_v.

Table S8. Statistics for Correlations between values of $\Delta\Delta J°_{b\text{-}mut}$ determined using ITC with values of $\Delta\Delta J°_{b\text{-}mut}$ estimated from WaterMap calculations.

Variable	$\Delta\Delta H°_b$	$-T\Delta\Delta S°_b$	$\Delta\Delta G°_b$	$\Delta\Delta J°_{b\text{-}WM}$ -$\Delta\Delta J°_b$	$\Delta SASA_{bind\text{-}ligand}$
Corr. coefficient (r)	0.893	0.662	0.47	0.75	0.6
Degrees of freedom (ν)	14	14	14	14	5
t-statistic	7.405	3.309	2.008	4.223	1.848
Two-tailed probability	<0.0001	0.005	0.064	0.001	0.124

Table S9

Mutant	*Global (Å)*	*Binding Pocket (Å)*[*]
3S73	0.00	0.00
F131W-BTA	0.23	0.14
V121I-BTA	0.21	0.13
L198A-BTA	0.23	0.16
T199S-BTA	0.23	0.11
V121T-BTA	0.23	0.13
F131Y-BTA	0.23	0.10
V121T/N67Q-BTA	0.21	0.13
V121T/F131Y-BTA	0.23	0.10
F131Y/L198A-BTA	0.23	0.14
F131Y/L198A-TA	0.21	0.14

[*]Alignment of residues within 6 Å of the position of BTA in the wild-type HCAII-BTA complex (i.e., crystal 3S73).

Supplementary References

[1] D. W. Christianson, C. A. Fierke, *Acc. Chem. Res.* **1996**, *29*, 331–339.

[2] P. W. Snyder, J. Mecinovic, D. T. Moustakas, S. W. Thomas, M. Harder, E. T. Mack, M. R. Lockett, A. Heroux, W. Sherman, G. M. Whitesides, *Proc. Natl. Acad. Sci.* **2011**, *108*, 17889–17894.

[3] J. D. Chodera, D. L. Mobley, *Annu. Rev. Biophys.* **2013**, *42*, 121–42.

[4] J. Fox, K. Kang, W. Sherman, A. Heroux, G. Sastry, M. Baghbanzadeh, M. Lockett, G. Whitesides, *J. Am. Chem. Soc.* **2015**, *137*, 3859–3866.

[5] G. Winter, *J. Appl. Crystallogr.* **2010**, *43*, 186–190.

[6] P. D. Zwart, P. H., Grosse-Kunstleve, R. W., Adams, *CCP4 Newsl.* **2005**, *43*, 27–35.

[7] P. D. Adams, P. V. Afonine, G. Bunkóczi, V. B. Chen, I. W. Davis, N. Echols, J. J. Headd, L. W. Hung, G. J. Kapral, R. W. Grosse-Kunstleve, et al., *Acta Crystallogr. Sect. D Biol. Crystallogr.* **2010**, *66*, 213–221.

[8] A. J. McCoy, R. W. Grosse-Kunstleve, P. D. Adams, M. D. Winn, L. C. Storoni, R. J. Read, *J. Appl. Crystallogr.* **2007**, *40*, 658–674.

[9] P. V Afonine, R. W. Grosse-Kunstleve, N. Echols, J. J. Headd, N. W. Moriarty, M. Mustyakimov, T. C. Terwilliger, A. Urzhumtsev, P. H. Zwart, P. D. Adams, *Acta Crystallogr. D. Biol. Crystallogr.* **2012**, *68*, 352–67.

[10] P. Emsley, K. Cowtan, *Acta Crystallogr. Sect. D Biol. Crystallogr.* **2004**, *60*, 2126–2132.

[11] I. W. Davis, A. Leaver-Fay, V. B. Chen, J. N. Block, G. J. Kapral, X. Wang, L. W. Murray, W. B. Arendall, J. Snoeyink, J. S. Richardson, et al., *Nucleic Acids Res.* **2007**, *35*, 375–383.

[12] G. Madhavi Sastry, M. Adzhigirey, T. Day, R. Annabhimoju, W. Sherman, *J. Comput. Aided. Mol. Des.* **2013**, *27*, 221–234.

[13] J. L. Banks, H. S. Beard, Y. Cao, A. E. Cho, W. Damm, R. Farid, A. K. Felts, T. A. Halgren, D. T. Mainz, J. R. Maple, et al., *J. Comput. Chem.* **2005**, *26*, 1752–1780.

[14] T. Beuming, R. Farid, W. Sherman, *Protein Sci.* **2009**, *18*, 1609–1619.

[15] T. Beuming, Y. Che, R. Abel, B. Kim, V. Shanmugasundaram, W. Sherman, *Proteins Struct. Funct. Bioinforma.* **2012**, *80*, 871–883.

[16] D. D. Robinson, W. Sherman, R. Farid, *ChemMedChem* **2010**, *5*, 618–627.

[17] K. J. Bowers, E. Chow, H. X. H. Xu, R. O. Dror, M. P. Eastwood, B. A. Gregersen, J. L. Klepeis, I. Kolossvary, M. A. Moraes, F. D. Sacerdoti, et al., *ACM/IEEE SC 2006 Conf.* **2006**, DOI 10.1109/SC.2006.54.

[18] G. A. Kaminski, R. A. Friesner, J. Tirado-Rives, W. L. Jorgensen, *J. Phys. Chem. B* **2001**, *105*, 6474–6487.

[19] W. L. Jorgensen, D. S. Maxwell, J. Tirado-Rives, *J. Am. Chem. Soc.* **1996**, *118*, 11225–11236.

[20] D. Shivakumar, J. Williams, Y. Wu, W. Damm, J. Shelley, W. Sherman, *J. Chem. Theory Comput.* **2010**, *6*, 1509–1519.

[21] T. Young, R. Abel, B. Kim, B. J. Berne, R. A. Friesner, *Proc. Natl. Acad. Sci. U. S. A.* **2007**, *104*, 808–813.

[22] R. Abel, T. Young, R. Farid, B. J. Berne, R. A. Friesner, *J. Am. Chem. Soc.* **2008**, *130*, 2817–2831.

[23] H. Beard, A. Cholleti, D. Pearlman, W. Sherman, K. a. Loving, *PLoS One* **2013**, *8*, 1–11.

[24] R. a. Friesner, J. L. Banks, R. B. Murphy, T. a. Halgren, J. J. Klicic, D. T. Mainz, M. P. Repasky,

E. H. Knoll, M. Shelley, J. K. Perry, et al., *J. Med. Chem.* **2004**, *47*, 1739–1749.

[25] T. a. Halgren, R. B. Murphy, R. a. Friesner, H. S. Beard, L. L. Frye, W. T. Pollard, J. L. Banks, *J. Med. Chem.* **2004**, *47*, 1750–1759.

[26] J. L. Devore, *Probability and Statistics for Engineering and the Sciences*, 2009, 8th Ed.

[27] T. P. Hopp, K. R. Woods, *Proc. Natl. Acad. Sci. U. S. A.* **1981**, *78*, 3824–3828.

[28] A. A. Zamyatnin, *Prog. Biophys. Mol. Biol.* **1972**, *24*.